Talanta 101 (2012) 122–127

Contents lists available at SciVerse ScienceDirect

Talanta

journal homepage: www.elsevier.com/locate/talanta

A rapid colorimetric detection method of trace Cr (VI) based on the redox etching of Ag_{core}–Au_{shell} nanoparticles at room temperature

Junwei Xin [a,b], Fuqiang Zhang [a], Yuexia Gao [a], Yanyan Feng [a], Shougang Chen [b,*], Aiguo Wu [a,*]

[a] Key Laboratory of Magnetic Materials and Devices, Division of Functional Materials and Nanodevices, Ningbo Institute of Materials Technology and Engineering, Ningbo 315201, China

[b] Institute of Materials Science and Engineering, Ocean University of China, Qingdao 266100, China

ARTICLE INFO

Article history:
Received 30 June 2012
Received in revised form
2 September 2012
Accepted 8 September 2012
Available online 16 September 2012

Keywords:
Colorimetric
Cr (VI)
Redox etching
Ag_{core}–Au_{shell} nanoparticles
Room temperature

ABSTRACT

A rapid colorimetric detection method of trace Cr (VI) in aqueous solutions has been developed based on non-aggregated Ag_{core}–Au_{shell} nanoparticles. It is based on the fact that Cr (VI) redox etches Ag_{core}–Au_{shell} nanoparticles at the present of bromide ions of hexadecyl trimethyl ammonium bromide (CTAB). The etching process of Ag_{core}–Au_{shell} nanoparticles would lead to a blue shift in the surface plasmon resonance (SPR) absorption peak as the size of Ag_{core}–Au_{shell} nanoparticles decreased. This colorimetric strategy based on size and component dependence of core-shell nanoparticles during the etching process provided a highly sensitive and selective detection method toward Cr (VI). Compared with other detection methods, this method provided a wide linear detection range from 1×10^{-8} M to 8×10^{-6} M over one order of magnitude, also has some practical capability. The cost-effective probe in this colorimetric method allowed rapid and sensitive detection of trace Cr (VI) ions as low as 1.0×10^{-7} M based on the observations by the naked eyes and 1.0×10^{-8} M based on the measurements of UV–vis spectra in aqueous solutions at room temperature. According to the preliminary data, it indicated that the current method showed very promising practical applicability for the determination of Cr (VI) in real environmental samples.

© 2012 Elsevier B.V. All rights reserved.

1. Introduction

In natural environment, chromium is generally in two most stable states of Cr (III) and Cr (VI), but their toxicities and mobilities differ significantly. On one hand, it is well known that Cr (III) participates in the metabolism of sugar and adipose in human beings and its deficiency may induce hyperglycemia, fat metabolism disorders, atherosclerosis, and coronary heart disease so on. [1,2] Moreover, chromium (III) is one of the essential trace elements in the human body and some chromium (III) compounds such as chromium (III) picolinate have been employed as supplemental or alternative medication for diabetes. [3] On the other hand, Cr (VI) is known to be highly soluble and toxic with carcinogenic effects, which is hazardous to human beings. [4] Therefore, much more attention has been attracted to the detection of Cr (VI) in a number of industrial processes such as chrome planting, dye and pigment fabrication, leather tanning, and wood preserving in recent years. Various sensor systems have been reported before.[5–13] Recently, a system performed by directed assembly of gold nanoparticles using DNA as a colorimetric sensor for the detection of metal ions has made a remarkable progress. [14,15] However, most of these systems have either limitations with aspect to sensitivity, simplicity or the need of surface modification for substantial selectivity. Also, a non-aggregation based label-free colorimetric sensor for the detection of Cr (VI) has been developed based on the redox etching of gold nanorods, [16a] but the method for preparation of gold nanorods is complicated, time-consuming, need of heating, and hard to control the aspect ratio of gold nanorods. Moreover, the detection of Cr (VI) based on the redox etching of gold nanorods is not suitable at room temperature. Above all, each of these strategies has advantages and disadvantages and no single method has gained supremacy.

In this report, a rapid colorimetric method for the detection of trace Cr (VI) in aqueous solutions based on label-free and non-aggregation Ag_{core}–Au_{shell} nanoparticles has been developed at room temperature. This rapid and simple method is based on the fact that Cr (VI) redox can etch Ag_{core}–Au_{shell} nanoparticles when there are bromide ions in hexadecyl trimethyl ammonium bromide (CTAB). The difference in the thickness of gold shell nanostructures caused a change of the surface plasmon resonance (SPR) absorption in the UV–vis spectra. The regular changes of the SPR absorption in the UV–vis spectra were used for quantitative analysis in the detection of Cr (VI). It was found that this colorimetric assay method for the detection limit of Cr (VI) concentration was as low as 1.0×10^{-7} M based on the observations by the naked eyes and 1.0×10^{-8} M based on the measurements of UV–vis spectra. The linear relationship of the quantitative analysis for Cr (VI) concentrations ranged from 8.0×10^{-6} to 1.0×10^{-8} M. This work exhibits very high sensitivity and excellent selectivity in the detection of Cr (VI) along with low

* Corresponding authors. Tel.: +86 574 86685039; fax: +86 574 86685163.
E-mail addresses: sgchen@ouc.edu.cn (S. Chen), aiguo@nimte.ac.cn (A. Wu).

0039-9140/$ - see front matter © 2012 Elsevier B.V. All rights reserved.
http://dx.doi.org/10.1016/j.talanta.2012.09.009

detection limit in aqueous solutions at room temperature. A real sample was tested to prove our method with the practicability for the environmental samples in aqueous solutions.

2. Experimental section

2.1. Materials and characterization

$HAuCl_4 \cdot 3H_2O$ (> 99.0%), $AgNO_3$ (≥ 99.8%), $NaBH_4$ (≥ 96.0%), trisodium citrate dihydrate ($C_6H_5Na_3O_7 \cdot 2\,H_2O$, ≥ 99.0%), $NH_2OH \cdot HCl$ (≥ 98.5%), hexadecyl trimethyl ammonium bromide (CTAB, 99%), and other reagents (analytical-reagent grade) were purchased from Sinopharm Chemical Reagent Co. Ltd (Shanghai, China) without further purification as received. Transmission electron microscopy (TEM) was performed using a Tecnai F20 instrument operated at 200 kV. UV–vis spectroscopy was performed using a Lambda 950 instrument and inductively coupled plasma atomic emission spectroscopy (ICP-AES) was performed with an Optima 2100 instrument from Perkin Elmer. Nanopure deionized and double distilled water (18.2 MΩ) was used for all experiments.

2.2. Synthesis of Ag_{core}–Au_{shell} nanoparticles

Ag_{core}–Au_{shell} nanoparticles were prepared according to the seed growth method of Cui et al. in a previous report with modification [17]. A batch of 100 mL solution with a final concentration of 0.2 mM $AgNO_3$ and 0.5 mM $C_6H_5Na_3O_7 \cdot 2H_2O$ in water was prepared. While stirring vigorously, 1.0 mL of 100 mM $NaBH_4$ was added drop by drop into the mixture and the solution was kept at room temperature for 2 h. After that, the core-shell nanoparticles with varying molar fractions of Au were prepared by the following method: x mL of 62.5 mM $NH_2OH \cdot HCl$ and x mL of 5 mM $HAuCl_4$ were added dropwise (ca. 2 mL/min) by two separated pipettes into the silver colloid solutions (where x is the concentration of Au desired in the final product). Stirring was continued for another 45minutes. The obtained Ag_{core}–Au_{shell} nanoparticles solution was centrifugated at 10,000 rpm for 15 min and then resuspended in 0.1 M CTAB with half of the original volume for use according to previous methods [18,19].

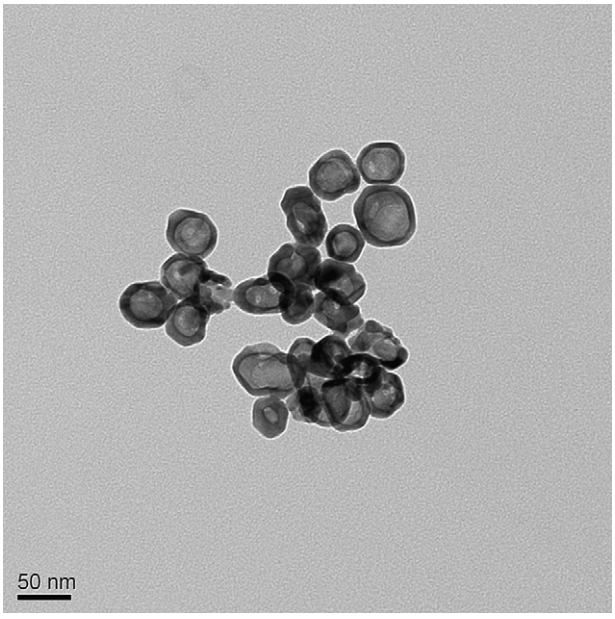

Fig. 1. TEM images of Ag_{core}–Au_{shell} nanoparticles. The molar ratio of Au/Ag was 1.25.

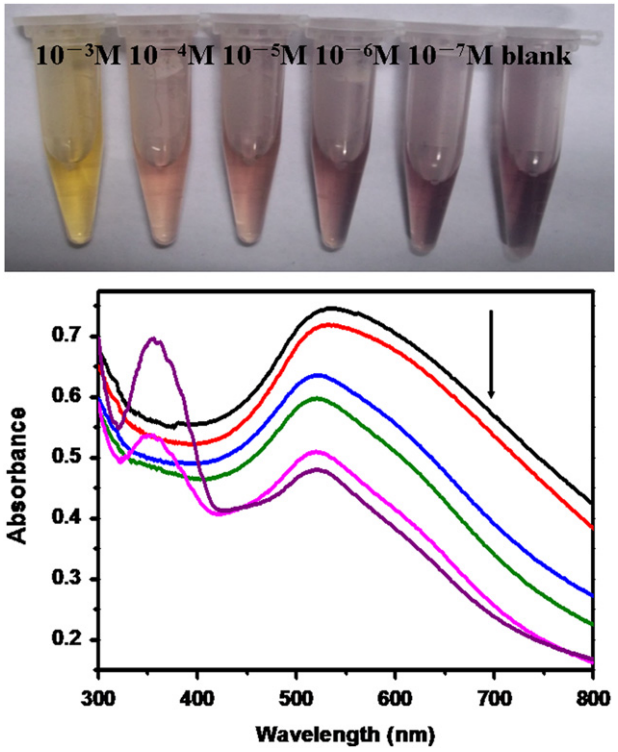

Fig. 2. (Top) Photographic images and (Bottom) surface plasmon resonance absorption change of Ag_{core}–Au_{shell} nanoparticles in the presence of different concentrations of Cr (VI). (1) 0 M, (2) 10^{-7} M, (3) 10^{-6} M, (4) 10^{-5} M, (5) 10^{-4} M, (6) 10^{-3} M (0.2 M CTAB; pH=2.00).

According to transmission electron microscopy data as shown in Fig. 1, Ag_{core}–Au_{shell} nanoparticles with the molar ratios of Au to Ag (1.25) were prepared.

2.3. Ag_{core}–Au_{shell} nanoparticles solution for the detection of Cr (VI)

For the detection of Cr (VI) by using the Ag_{core}–Au_{shell} nanoparticles solution, different concentrations of Cr (VI) in aqueous solutions were added separately to a 2.0 mL of solution containing Ag_{core}–Au_{shell} nanoparticles, and adjusted the pH value of the mixtures to 2.0. As shown in Fig. 2, the mixtures were maintained at room temperature for only several minutes, and then the color changed from violet to yellow quickly.

3. Results and discussion

3.1. Sensing strategy

To understand the role that Cr (VI) plays in the redox etching of Ag_{core}–Au_{shell} nanoparticles, the SPR absorption of Ag_{core}–Au_{shell} nanoparticles was monitored under conditions of varying Cr (VI) concentrations shown in Fig. 2. The initial Ag_{core}–Au_{shell} nanoparticles exhibited the SPR absorption peak located at 535 nm and the SPR absorption peak gradually blue shifted and the absorbance decreased as the concentration of Cr (VI) increased. Moreover, a new SPR absorption peak was observed about 350–380 nm when the concentration of Cr (VI) reached to 10^{-4} M. This is the evidence of silver nanoparticles after the redox etching of Ag_{core}–Au_{shell} nanoparticles. Before Li et al. had also investigated the change of the absorption properties/selectivity of silver nanoparticles after complete etching/leaching of Au from the surface of Ag/Au nanoparticles by thiosulfate ($S_2O_3^{2-}$), it proves the data in our experimental.[16b] Besides the color of

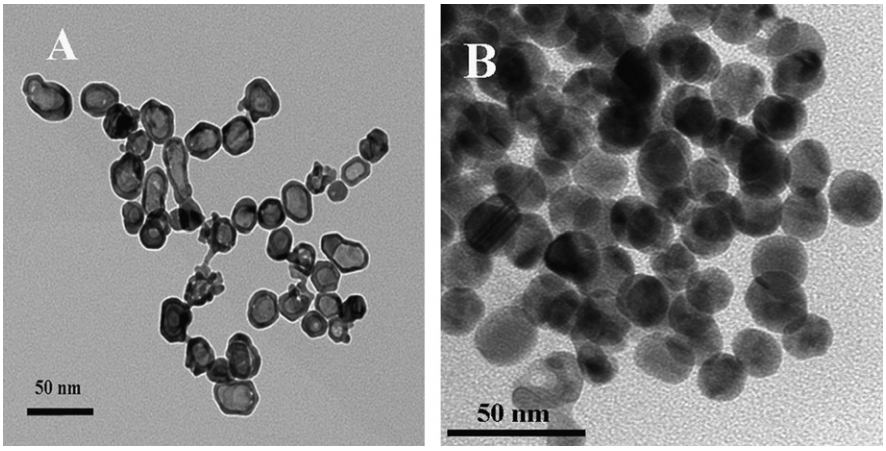

Fig. 3. TEM images of Ag_{core}–Au_{shell} nanoparticles in the presence of different concentrations of Cr (VI). (A) 0 M, (B) 10^{-3} M (0.2 M CTAB; pH=2.00).

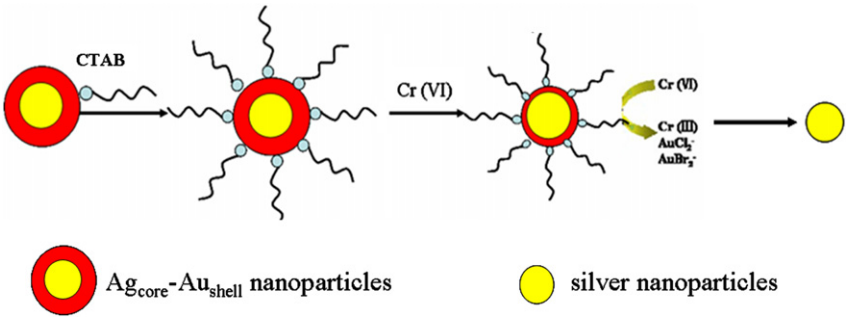

Scheme 1. Schematic illustration on the redox etching mechanism of the Ag_{core}–Au_{shell} nanoparticles induced by Cr (VI).

Ag_{core}–Au_{shell} nanoparticles solutions distinctly changed from violet to yellow. Taking into account of these observations and with regards to the investigations, it was shown that the blue-shift was due to the decreasing of particle size of Ag_{core}–Au_{shell} nanoparticles, which agreed very well with the TEM images shown in Fig. 3.

Scheme 1 illustrated on a redox etching mechanism of the Ag_{core}–Au_{shell} nanoparticles induced by Cr (VI), which is employed in this method. A blue shift of the SPR wavelength is due to the decreasing of the size of Ag_{core}–Au_{shell} nanoparticles, when the Ag_{core}–Au_{shell} nanoparticles reacted with Cr (VI) in aqueous solutions. The standard electron potential of Au (I)/Au (0) and Ag (I)/Ag (0) is 1.691 eV and 0.7966 eV, respectively. The electron potential of Au (I)/Au (0) and Ag (I)/Ag (0) decreases when the concentrations of Br^- of CTAB and Cl^- of HCl increase, and they act as ligands of Ag_{core}–Au_{shell} nanoparticles ($AuBr_2^- + e^- \rightarrow Au + 2Br^-$, $E=0.959$ eV,[20] $AuCl_2^- + e^- \rightarrow Au + 2Cl^-$, $E=1.15$ eV,[21] $AgBr + e^- \rightarrow Ag + Br-$, $E=0.07133$ eV, $AgCl + e^- \rightarrow Ag + Cl^-$, $E=0.22233$ eV). The standard electron potential of Cr (VI)/Cr (III) (1.33 eV) is higher than that of Au (I)/Au (0) and Ag (I)/Ag (0) in the presence of Br^- and Cl^- ions, which enables Cr (VI) to oxidize Ag_{core}–Au_{shell} nanoparticles. The redox etching process induced by Cr (VI) causes a significant decrease for the thickness of gold shell. When the concentration of Cr (VI) reached a higher level, upon further oxidation, the size of Ag_{core}–Au_{shell} nanoparticles decreased, and the core-shell nanoparticles converted into silver nanospheres along with eventually completely oxidization, which exhibited different color to change from violet to yellow.

3.2. Optimization of the conditions for Cr (VI) measurement

In order to optimize the conditions for the determination of Cr (VI), a number of parameters that influence on the sensitivity, selectivity, accuracy and stability were investigated in a univariate approach.

(1) *Effects of the thickness and size of Ag_{core}–Au_{shell} nanoparticles*
The thickness and concentration of Ag_{core}–Au_{shell} nanoparticles in the detection system were examined in order to obtain a wide linear range and high sensitivity. Fig. S1 showed the TEM images of Ag_{core}–Au_{shell} nanoparticles with different thickness. Moreover, Au/Ag composite nanoparticles were generated with the increased amount of $HAuCl_4 \cdot 3H_2O$, and it would affect the detection limit of Cr (VI) (shown in Fig. S2). From these pictures, sample D (shown in Fig. S2) showed a clearly core-shell structure of Au and Ag with the molar ratio of 1.25. The lower the concentration of Ag_{core}–Au_{shell} nanoparticles, the redox etching rate of Ag_{core}–Au_{shell} nanoparticles induced by Cr (VI) increased and blue shift accordingly enhanced, with a favorable sensitivity but narrow linear range compared with high concentration of Ag_{core}–Au_{shell} nanoparticles. In contrast, higher concentration of Ag_{core}–Au_{shell} nanoparticles expanded the linear range but limited the sensitivity. In consideration of both linear range and sensitivity, 3.6×10^{-4} M of silver atoms in Ag_{core}–Au_{shell} nanoparticles were chosen. In the first step of the reaction, excessive $NaBH_4$ was added, therefore, $AgNO_3$ was completely transformed into silver nanoparticles. As shown in Fig. 1, Ag_{core}–Au_{shell} nanoparticles were well prepared in the TEM image. Given all that, the concentration of Ag_{core}–Au_{shell} nanoparticle solution can be calculated from the amount of silver nitrate.

(2) *Effects of pH and CTAB*
As we all know that the redox etching rate of Ag_{core}–Au_{shell} nanoparticles enhanced as the pH value decreased[16a], which ascribed to the electron potential and oxidation capability of Cr (VI) increased. To support this point, simple calculations were conducted to roughly estimate the electron potentials of

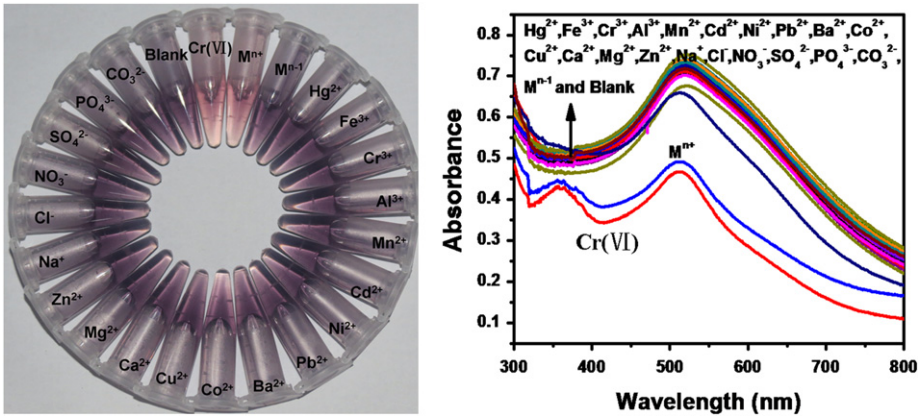

Fig. 4. (Left) Photographic images and (Right) the UV–vis spectra of Ag_{core}–Au_{shell} nanoparticles in the presence of different metal ions (50 μM). Especially M^{n+} contains all of the ions (50 μM) and M^{n-1} contains all of the above interfering ions (50 μM) with the exception of Cr (VI) at pH=2.00.

Cr (VI) at different pH values. Because there was little Cr (III) at the beginning, it was reasonable to assume that only 0.01% of Cr (VI) turned into the reductive species of Cr (III) for the calculation of the initial electron potential. Then, it was found that the electron potentials of Cr (VI)/Cr (III) were 1.271 and 0.995 eV when the pH values were 1.0 and 3.0, respectively. Besides, the increasing Cl^- in the solution could further reduce the electron potential of the gold and silver species and facilitate the redox etching of Ag_{core}–Au_{shell} nanoparticles. However, the Ag_{core}–Au_{shell} nanoparticles were not stable in one hour when the pH of the aqueous solution was less than 1.00. And the color did not change obviously even if the concentration of Cr (VI) was 10^{-5} M when the pH of the aqueous solution was higher than 3.00. As for the detail, effects of pH for the detection of Cr (VI) are shown in Fig. S5 in supporting information. Moreover, CTAB could effectively absorb on the surface of the Ag_{core}–Au_{shell} nanoparticles, which is supposed to prevent chemical etching process as the considerable amount of Br^- introduced from CTAB that reduces the electron potential of the gold and silver species ($AuBr_2^- + e^- \rightarrow Au + 2Br^-$, $E=0.959$ eV, $AgBr + e^- \rightarrow Ag + Br-$, $E=0.07133$ eV). However, a further increase of CTAB concentration leads to an increased interference from other oxidative cations, which lowers the detection selectivity of Cr (VI). As for the detail, effects of CTAB concentration for the detection of Cr (VI) are shown in Fig. S6 in supporting information. Above all, it was the reason why the concentration of CTAB was 0.1 M and the pH of the aqueous solution at 2.0 were used in this experiment. Under these optimized conditions, the recognition of Cr (VI) with Ag_{core}–Au_{shell} nanoparticles showed a significant color change by this colorimetric assay method.

3.3. Selectivity and sensitivity for Cr (VI)

In order to study the influence of other metal ions on Cr (VI) redox etching of Ag_{core}–Au_{shell} nanoparticles, competitive experiments were carried out in the presence of Cr (VI) (50 μM) with Hg^{2+}, Fe^{3+}, Cr^{3+}, Al^{3+}, Mn^{2+}, Cd^{2+}, Ni^{2+}, Pb^{2+}, Ba^{2+}, Co^{2+}, Cu^{2+}, Ca^{2+}, Mg^{2+}, Zn^{2+}, Na^+, Cl^-, NO_3^-, SO_4^{2-}, PO_4^{3-}, and CO_3^{2-} at 50 μM, respectively (As for influence of potentially interfering ions, i.e. tolerance ratios, the data was summarized in Table S1). Fig. 4 showed that the photographic images and UV–vis spectra of Ag_{core}–Au_{shell} nanoparticles when various types of metal ions were added to Ag_{core}–Au_{shell} nanoparticles in aqueous solutions within one minute, it was clearly shown that only the sample was added Cr (VI), which induced a distinct color change from violet to yellow (Fig. 4, left image). Moreover, Cr (VI) was also the only ion which resulted in an absorption peak blue shift from 535 nm to about 370 nm (Fig. 4, right image). The blue shift was also observed as a color change from violet to yellow. These results could be evidences for the redox etching process of Ag_{core}–Au_{shell} nanoparticles that was triggered by Cr (VI), which agreed very well with the TEM images shown in Fig. S3. Most importantly, this finding could be a basis for the detection of Cr (VI) with Ag_{core}–Au_{shell} nanoparticles as even if all of the above interfering ions except Cr (VI) were added that did not influence the detection of Cr (VI). It was suggested that this method could be suitable for the detection of Cr (VI) in various types of environmental samples.

Under these optimized conditions, the Ag_{core}–Au_{shell} nanoparticles were utilized for the colorimetric assay of Cr (VI). As shown in Fig. 2, various colors of the Ag_{core}–Au_{shell} nanoparticles aqueous solutions have been seen after the addition of different concentrations of Cr (VI). As incorporating the concentration of Cr (VI) increased from 10^{-7} M to 10^{-3} M, the color of the aqueous solutions gradually changed from violet to yellow. The color change could be clearly observed when the concentration of Cr (VI) was higher than 1.0×10^{-7} M shown in Fig. 2, in other words, the detection limit of Cr (VI) was about 1.0×10^{-7} M according to this approach of colorimetric assay by the naked eyes. Moreover, the UV–vis spectroscope allowed the detection of low concentrations of Cr (VI) for the quantitative assay. A wide range of Cr (VI) concentration from 0.001 μM to 100 μM could be successfully detected out in the experiments (shown in Fig. S4). As shown in Fig. 5A, the surface plasmon resonance absorption of Ag_{core}–Au_{shell} nanoparticles gradually blue shifted as the concentration of Cr (VI) increased which was triggered by the redox etching of Ag_{core}–Au_{shell} nanoparticles and decreased their particles' size, which agreed very well with the TEM images shown in Fig. S3. Above all, a good linear relationship ($R=0.99776$) in the range of the concentrations of Cr (VI) from 0.01 μM to 8 μM was obtained by A_0/A at 526 nm shown in Fig. 5B. Furthermore, the color of Ag_{core}–Au_{shell} nanoparticles solution was changed in the presence of 2 μM Cr (VI) was within 5 min shown in Fig. 6 at room temperature. It means a rapid method for detection of Cr (VI) in aqueous solutions.

Moreover, the control experiments of Br ions and Cl ions for Cr (VI) detection was also investigated and the data was shown in Fig. 6S in Supporting Information part.

4. Application of Ag_{core}–Au_{shell} nanoparticles for the analysis of real environment water samples

To confirm the practical application capability of Ag_{core}–Au_{shell} nanoparticles, the concentration of Cr (VI) in real water samples

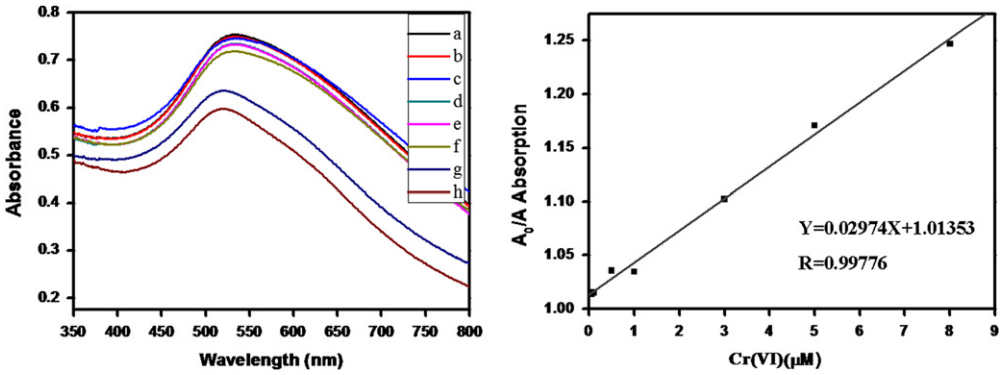

Fig. 5. (A) Surface plasmon resonance absorption changes of Ag_{core}–Au_{shell} nanoparticles in the presence of different concentrations of Cr (VI). (a) 0 μM, (b) 0.01 μM, (c) 0.05 μM, (d) 0.1 μM, (e) 0.5 μM, (f) 1 μM, (g) 5 μM, (h) 8 μM. (B) The calibration curve for the detection of Cr (VI) by Ag_{core}–Au_{shell} nanoparticles. The ratio (A_0/A) was plotted against different concentrations of Cr (VI). Where A_0 is the UV absorption of the Ag_{core}–Au_{shell} nanoparticles and A is the UV absorption of the Ag_{core}–Au_{shell} nanoparticles in the presence of different concentrations of Cr (VI) at 526 nm.

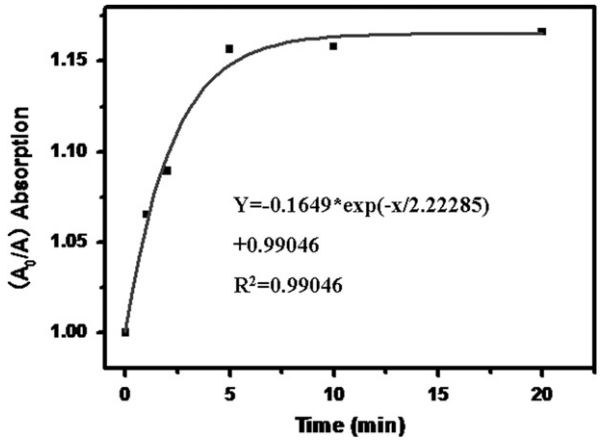

Fig. 6. The redox etching time of Ag_{core}–Au_{shell} nanoparticles in the presence of Cr (VI) (2 μM) at room temperature.

(from Ningbo Environment Monitoring Center, Ningbo, China) was determined by applying this assay method. First, the pH of real water samples was adjusted to 9.0 with a certain amount of ammonia to precipitate Cr^{3+} and stirred for 30 min at room temperature. Then the pH values of the treated water samples were adjusted to 2.0 with HCl before use. A calibration curve of Ag_{core}–Au_{shell} nanoparticles SPR shifts in the presence of different concentrations of Cr (VI) was prepared (see Fig. 5B). The concentration of Cr (VI) in the real water samples (from Ningbo Environment Monitoring Center, Ningbo, China) was from 1.60 μM to 1.75 μM based on the detection results, which was generally in good agreement with the detection result of Cr (VI) (1.63 μM) by the ICP-AES-based method. Thus, the result demonstrated that the currently designed colorimetric method is applicable for the detection of Cr (VI) in real environmental water samples.

5. Conclusions

A highly sensitive and selective colorimetric sensor is designed for the rapid detection of Cr (VI) at room temperature based on the redox etching process of non-aggregated Ag_{core}–Au_{shell} nanoparticles which is induced by Cr (VI). Cr (VI) was the only metal ion which brought a color change of the sample solution from violet to yellow and decreased the absorption of the SPR with Ag_{core}–Au_{shell} nanoparticles. The optimal pH value of Ag_{core}–Au_{shell} nanoparticles solution was determined to be 2.0. In comparison with aggregation based colorimetric sensor based on cross-linking or electrostatic absorption, the proposed non-aggregation colorimetric sensor shows high selective and sensitive response towards Cr (VI) without surface modification. Some tests of the Cr (VI) concentration with the real water sample were done and the results were consistent with the ICP-AES-based method. In principle, this method could provide a promising sensor to on-line rapidly detecting Cr (VI) in real water samples.

Acknowledgments

This work was supported by the Program of Zhejiang Provincial Natural Science Foundation of China under Grant No. R5110230, Natural Science Foundation of China under Grant No. 31128007; Hundred Talents and Academy-Locality Cooperation Programs of Chinese Academy of Sciences, and Ningbo Science and Technology Bureau (Grants Nos. 2011C50009, and 2009B21005), the CAS/SAFEA International Partnership Program for Creative Research Teams. And the Projects Sponsored by the Scientific Research Foundation for the Returned Overseas Chinese Scholars, States of Ministry of Human Resources & Social Security. The authors also thank Prof. Yanbo Weng and Dr. Xiaoqin Fu from Ningbo Environment Monitoring Center, Ningbo, China for the real environmental samples.

Appendix A. Supporting information

Supplementary data associated with this article can be found in the online version at http://dx.doi.org/10.1016/j.talanta.2012.09.009.

References

[1] H.G. Preuss, B. Echard, N.V. Perricone, D. Bagchi, T. Yasmin, S.J. Stohs, J. Inorg. Biochem. 102 (2008) 1986–1990.
[2] M.F. Mccarty, Med. Hypotheses. 41 (1993) 316–324.
[3] C.L. Broadhurst, P. Domenico, Diabetes. Technol. The 8 (2006) 677–687.
[4] Health assessment document for chromium (review Draft); Environmental Protection Agency: Springfield, VA, 1983.
[5] E. Margui, C. Fontas, M. Toribio, M. Guillem, M. Hidalgo, I. Queralt, Appl. Spectrosc. 64 (2010) 547–551.
[6] Z.Q. Han, L. Qi, G.Y. Shen, W. Liu, Y. Chen, Anal. Chem. 79 (2007) 5862–5868.
[7] O.D. Uluozlu, M. Tuzen, D. Mendil, B. Kahveci, M. Soylak, J. Hazard. Mater. 172 (2009) 395–399.
[8] M.S. Hosseini, F. Belador, J. Hazard. Mater. 165 (2009) 1062–1067.
[9] Y. Xiang, L. Mei, N. Li, A.J. Tong, Anal. Chim. Acta. 581 (2007) 132–136.
[10] M.F. Bergamini, D.P. dos Santos, M.V.B. Zanoni, Sens. Actuat. B-Chem. 123 (2007) 902–908.
[11] M. Jakubowska, J. Hazard. Mater. 176 (2010) 540–548.
[12] H. Chen, P. Du, J. Chen, S.H. Hu, S.Q. Li, H.L. Liu, Talanta 81 (2010) 176–179.

[13] K. Sasaki, S. Oguma, Y. Namiki, N. Ohmura, Anal. Chem. 81 (2009) 4005–4009.
[14] Y. Lu, J.W. Liu, J. Li, P.J. Bruesehoff, C.M.B. Pavot, K.A. Brown, Biosens. Bioelectron. 18 (2003) 529–540.
[15] T. Lan, K. Furuya, Y. Lu, Chem. Commun. 46 (2010) 3896–3898.
[16] (a) F.M. Li, J.M. Liu, X.X. Wang, L.P. Lin, W.L. Cai, Y.N. Zeng, L.H. Zhang, S.Q. Lin, Sens. Actuat. B-Chem. 155 (2011) 817–822;
(b) T. Lou, L. Chen, Z. Chen, Y. Wang, L. Chen, J. Li, ACS Appl. Mater. Interfaces 11 (2011) 4215–4220.
[17] Y. Cui, B. Ren, J.L. Yao, R.A. Gu, Z.Q. Tian, J. Phys. Chem. B 110 (2006) 4002–4006.
[18] F.Q. Zhang, l.Y. Zeng, Y.X. Zhang, H.Y. Wang, A.G. Wu, Nanoscale 3 (2011) 2150–2154.
[19] F.Q. Zhang, L.Y. Zeng, C. Yang, J.W. Xin, H.Y. Wang, A.G. Wu, Analyst 136 (2011) 2825–2830.
[20] C.K. Tsung, X.S. Kou, Q.H. Shi, J.P. Zhang, M.H. Yeung, J.F. Wang, G.D. Stucky, J. Am. Chem. Soc. 128 (2006) 5352–5353.
[21] R.X. Zou, X. Guo, J. Yang, D.D. Li, F. Peng, L. Zhang, H.J. Wang, H. Yu, Cryst. Eng., Comm. 11 (2009) 2797–2803.